Comparison of the hot corrosion of nanostructured and microstructured thermal barrier coatings

C. H. Zhou, Z. Y. Zhang, Q. M. Zhang and Y. Li*

Thermal barrier coatings of nanostructured and microstructured yttria stabilized zirconia (YSZ) were deposited on GH4049 substrate by air plasma spray, respectively. Hot corrosion behaviors of both coatings were evaluated in comparative aspects. Results revealed that the nanostructured YSZ displayed higher resistance to the hot corrosion attack by Na_2SO_4 and V_2O_5. It was also shown, through X-ray diffraction quantitative phase analysis, that the nanostructured YSZ had good resistance to the tetragonal-monoclinic phase transformation during the hot corrosion process.

1 Introduction

Thermal barrier coatings (TBCs) are widely used in land-based, naval and aero-engine gas turbines owing to their higher operating efficiencies, longer service lifetime and less harmful emissions. Many researchers and engineers have summarized the materials, structures, and preparation of these coatings [1–8]. There are commonly four primary constituents in a TBC system. They are (i) the TBC itself, (ii) an aluminum containing bond coat (BC) between the substrate and the TBC, (iii) a thermally grown oxide (TGO) formed between the TBC and the BC, and (iv) the superalloy substrate. In the practical application, significant problems of the TBCs are the tendencies towards mechanical and chemical failures in the severe environment. To explore the failure mechanism of TBCs, many factors including TGO, thermal expansion misfit, interfacial roughness, and ceramic sintering have been investigated [9–13].

It is well known that the presence of monoclinic phase is negative for the application of TBCs owing to the tetragonal-monoclinic transformation accompanied with about 3–5% volume change [14]. Increasing yttria content up to 7–9 wt% can lower the tetragonal-monoclinic transformation temperature and thereby stabilize the tetragonal phase. Nevertheless, the tetragonal-monoclinic transformation still occurs owing to the depletion of yttria stabilizing agent induced by hot corrosion of molten salt [15, 16], such as sulfur and vanadium in low-quality fuels [17, 18]. Many laboratorial investigations have been carried out to explore the hot corrosion mechanism [15, 16, 19, 20], and furthermore, to improve hot corrosion resistance. The most promising approach is to substitute Y_2O_3 with more acidic stabilizer elements, such as CeO_2, In_2O_3, Sc_2O_3, $YTaO_4$, and dispersed Al_2O_3 [15, 21–25]. A laser-glazing method has also been developed to improve the surface microstructure of ceramic coating with the intention of preventing the molten salt penetrating into the zirconia coating [26]. However, there are several disadvantages of the aforementioned methods, e.g., lower thermal expansion coefficients, poor mechanical properties, and chemical reactions. Recently, nanocrystallization of the TBCs has been verified to be an efficient method to improve phase stabilization, thermal shock resistance, and mechanical properties [27–29]. Nevertheless, the mechanism of that nanostructured yttria stabilized zirconia (YSZ) improves hot corrosion resistance of TBCs is still not clear. The present work compared the hot corrosion processes of the nanostructured and microstructured YSZ at several intervals. The tetragonal-monoclinic transformation induced by hot corrosion was analyzed, aiming at exploring the hot corrosion mechanism of nanostructured YSZ.

2 Experimental materials and procedures

2.1 Materials and coating preparation

Thermal barrier coatings, composed of a bond coating and a top coating, were air-plasma-sprayed on a GH4049 alloy (0.04–0.1% C, 9.5–11.0% Cr, 14.0–16% Co, 5.0–6.0% W, 4.5–5.5% Mo, 3.7–4.4% Al, $\leq$1.5% Fe, 0.2–0.5% V, Ni balance, in weight) substrate. The substrate geometry was a square of $20 \times 20\,mm^2$ surface area with 3 mm thickness. The spraying material for the BC was microstructured NiCoCrAlY and the top coats were nanostructured and microstructured YSZ (ZrO_2-8 wt%Y_2O_3). The chemical composition and original particle size of BC and top coat are shown in Table 1. Prior to spraying process, the substrates were successively ground with SiC paper up to 800# (10 μm). They

C. H. Zhou
Postdoctoral Research State of Materials Science and Engineering, Harbin Institute of Technology, Harbin 150001 (P. R. China)

C. H. Zhou, Z. Y. Zhang, Y. Li
Center for Composite Materials and Structures, Harbin Institute of Technology, Harbin 150001 (P. R. China)
E-mail: liyao@hit.edu.cn

Q. M. Zhang
School of Chemical Engineering and Technology, Harbin Institute of Technology, Harbin 150001 (P. R. China)

Table 1. Chemical components and particle size of materials

Type of TBC		YSZ	Ni23Co20Cr9Al0.6Y (μm)	Abbreviation
Nanostructured	Layer thickness	250 μm	110	Nano-TBC
	Particle size	40–50 nm (before agglomeration)	110	
		20–80 μm (after agglomeration)		
Microstructured	Layer thickness	250 μm	110	Micro-TBC
	Particle size	40–60 μm	110	

were then cleaned by absolute ethyl alcohol in an ultrasonic set before grit blasted by alumina particles. Subsequently, the substrates were placed into the air plasma spray (APS) system (Switzerland PT Corporation, R-750 C) for overlaying with NiCoCrAlY bond coating. As the thermal expansion mismatch of YSZ, NiCoCrAlY, and Ni-cased superalloy, the substrate was preheated at 95 °C for 5 min prior to the spraying. Nanostructured and microstructured YSZ were sprayed onto as sprayed BC specimen in an APS system, respectively. The fabricated parameters of the coating process are given in Table 2.

Figure 1a and b are cross-sectional images of the as-sprayed TBCs, respectively. Both TBCs show typical characteristics, i.e., an outer ceramic coating, an intermediated layer of BC and the substrate of Ni-based superalloy. X-ray diffraction (XRD) patterns in Fig. 1c indicate that both coatings were composed of tetragonal phase and a small amount of monoclinic phase.

2.2 Hot corrosion tests

A mixture of 20 wt% Na_2SO_4 and 80 wt% V_2O_5 powders was selected as corrosive salt. Some physical properties of each salt have been presented [30]. These mixed salts were spread over the coatings in a concentration of about 2 mg/cm^2. Hot corrosion tests were performed in a box-type electric resistance furnace in air. The corrosion temperature was set at 900 °C in order to simulate the service environment for gas turbine. During the tests, three identical samples were directly placed into the furnace. After every hot corrosion test, the samples were furnace cooled to 200 °C in order to avoid the phase transformation induced by fast cooling, and then they were taken out and cooled down to room temperature in air. During the hot corrosion, the coatings were also periodically inspected about every 5 h to ensure the coatings were still covered by salts.

2.3 Microstructure and chemical analysis

The surface, cross-sectional morphologies and component were examined using a scanning electron microscope (SEM) equipped with an energy dispersive spectrometer (EDS). XRD tests were employed to determine the phase transformation of ceramic coating and the hot corrosion products.

Table 2. Processing parameters for spraying coatings

Parameter	Nano-YSZ	Micro-YSZ	NiCoCrAlY
Current (A)	550	550	450
Voltage (V)	57.3	57.3	57.3
Primary gas, Ar (L/min)	39	39	37
Secondary gas, H_2 (L/min)	7	8	2
Powder feed rate (g/min)	40	40	30
Spray distance (cm)	7	7	15

3 Results and discussion

3.1 Surface morphology and component analysis after hot corrosion

Figure 2 shows surface morphologies of both coatings corroded in the mixture salt of Na_2SO_4 and V_2O_5 at 900 °C for 60 and 100 h, respectively. Generally, the micro-TBC displays lower hot corrosion resistance than nano-TBC by observing the amount of corrosion products on the surface of TBCs. The evolution of corrosion morphology for micro-TBC is from worm-shaped to crystal rods in the 100 h of corrosion, which shows the growth of corrosion product in size. However, in the case of nano-TBC, it obviously implies that biaxial growth of columnar-shaped crystal is the main morphological evolution, as shown in Fig. 2c and d. In addition, the surface morphologies after hot corrosion in this work is different with other investigations [19, 30], which can be probably attributed to the difference in corrosion temperature and time. For example, the morphology of the corrosion products is either particle-like formed after 1 h of hot corrosion at 980 °C or rod-, dentritic-like generated after 40 h of corrosion at 1050 °C. In the present work, it can be seen that the corrosion products grew continuously by comparing their shapes and sizes at different corrosion time. Although this process is not witnessed *in situ*, it may also help us explore the principle of hot corrosion of YSZ. Since the hot corrosion of YSZ undergoes a nucleation stage and a growth process, the surface morphology obtained at different experimental conditions is probably different in nature. Nevertheless, the component of corrosion products is the same, i.e., YVO_4, which can be proved by the following EDS examination and XRD analysis.

Energy dispersive spectra in Fig. 3 detected from the points on the surface of the coatings in Fig. 2 (dotted arrows point out) demonstrates that all the corrosion products were mainly composed of yttrium, zirconium, vanadium, and oxygen. Only minor amount of sulfur as well as sodium were found in spite that the original corrosive salts of the mixture of 20 wt% Na_2SO_4 and 80 wt% V_2O_5 powders contained more Na_2SO_4. It implies that the corrosion process is mainly the reaction of V_2O_5 and YSZ, which is in accordance with the previous reports [15–17, 19, 30]. As the formation of ZrV_2O_7 is usually slow according to the equation: $ZrO_2 + V_2O_5 \rightarrow ZrV_2O_7$ [31], ZrV_2O_7 is not expected. The following XRD analysis identifies that the corrosion products

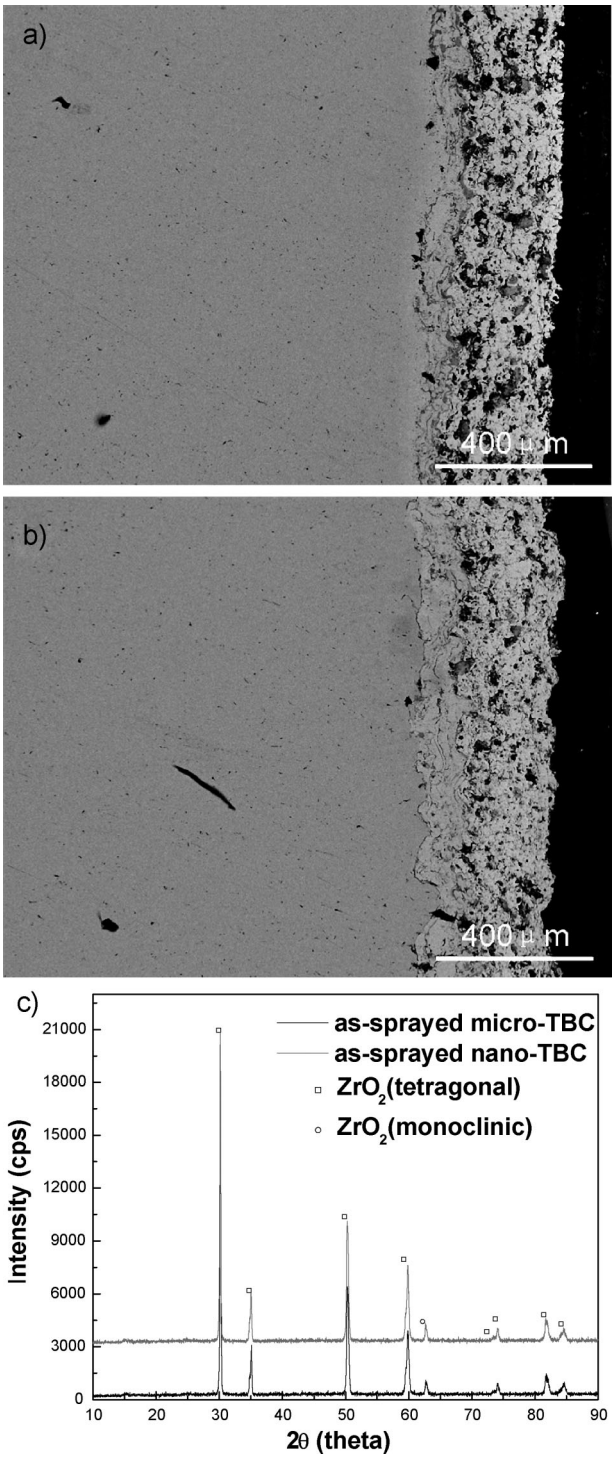

Figure 1. SEM cross-sectional micrographs of the as-sprayed coatings: (a) micro-TBC; (b) nano-TBC; (c) XRD patterns of as-sprayed coatings

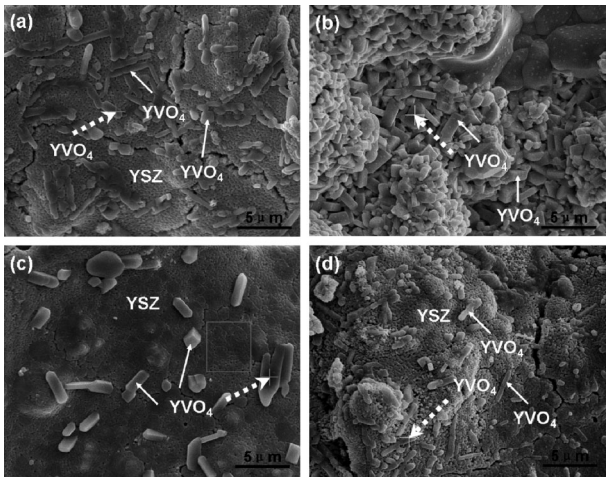

Figure 2. SEM micrographs show the surface morphology of coatings after hot corrosion: (a) micro-TBC, after 60 h of corrosion; (b) micro-TBC, after 100 h of corrosion; (c) nano-TBC, after 60 h of corrosion; (d) nano-TBC, after 100 h of corrosion

were YVO_4. The EDS spectrum from the rectangular area in Fig. 2c shows that the surface of coatings is still YSZ.

Figure 4 shows the XRD patterns of both coatings corroded for 60 and 100 h, respectively. As can be indexed, the corrosion products were YVO_4. Since the hot corrosion is not severe owing to the lower corrosion temperature of 900 °C and shorter corrosion time limited to 100 h, the XRD patterns witnessed peaks of YVO_4 are very weak and peaks of YSZ phase are strong. Nevertheless, combining the XRD analysis with the local EDS analysis in Fig. 3, it can be further identified that the corrosion products were YVO_4.

The mechanism of molten salt corrosion has been proposed after extensive investigations. The hot corrosion process can be explained by the following reactions [6, 7, 15–17, 30, 32, 33]:

$$V_2O_5 + Na_2SO_4 \rightarrow 2(NaVO_3) + SO_3 \quad (1)$$

$$ZrO_2(Y_2O_3) + 2(NaVO_3) \rightarrow ZrO_2(\text{monoclinic}) + 2YVO_4 + Na_2O \quad (2)$$

The below reaction can also directly occur [34]:

$$ZrO_2(Y_2O_3) + V_2O_5 \rightarrow ZrO_2(\text{monoclinic}) + 2YVO_4 \quad (3)$$

In the initial stage, $NaVO_3$ was formed after the reaction of V_2O_5 and Na_2SO_4 according to reaction (1) or the reaction (3). Then, $NaVO_3$ reacted with Y_2O_3 to form monoclinic ZrO_2, YVO_4, and Na_2O as the reaction (2) indicated. Through the EDS analysis performed on the different points or the mapping surface of the coatings, only a small amount of Na and S were detected or none. It seems that Na_2O was sublimated during hot corrosion tests, with regard to this result confirmed by other researchers [32, 35]. And S was emitted into air in the form of SO_3.

The corrosion resistance of nano-TBC is better than the micro-TBC, which can be attributed to that the nanostructure leads to lower defects, such as pores or cracks, excellent smooth surface and component homogeneity [6, 36–38]. Under the corrosive conditions, it is more difficult for the molten salt to penetrate into zirconia coating in nano-TBC than in micro-TBC.

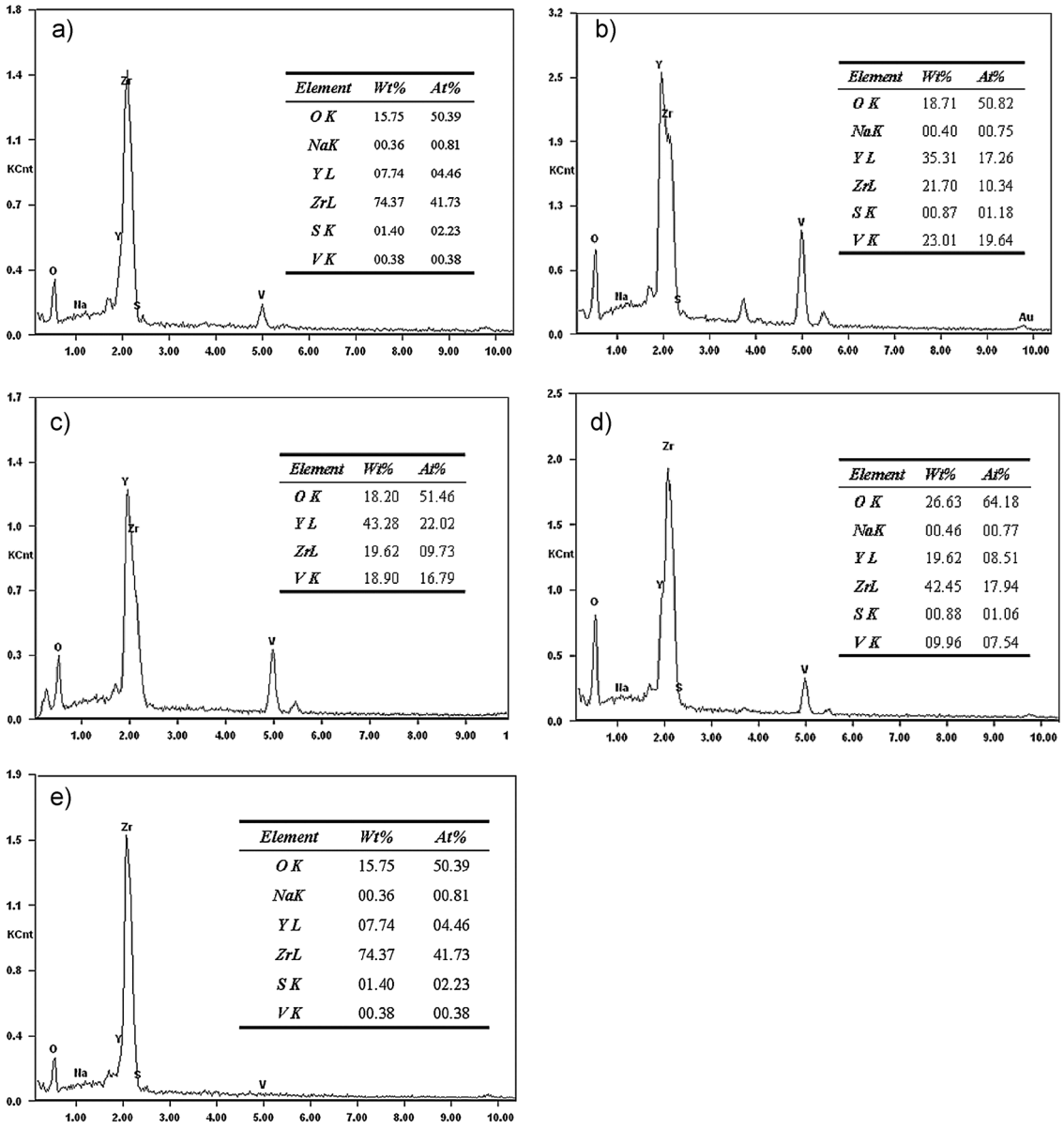

Figure 3. EDS spectra from the points on the surface of the coatings in Fig. 2 reveal the corrosion products pointed out by dotted arrow: (a) micro-TBC, after 60 h of corrosion; (b) micro-TBC, after 100 h of corrosion; (c) nano-TBC, after 60 h of corrosion; (d) nano-TBC, after 100 h of corrosion and (e) EDS spectrum form the rectangular area in Fig. 2c

The corrosion process only occurs on the near surface of zirconia coating. As the state of surface coating is homogeneous, the initial corrosion generates at local areas where surface defects exist. Therefore, the hot corrosion of nano-TBC shows a point corrosion model. After a long corrosion time, the initial corrosion nuclei biaxially grow and the growth penetrating into the zirconia coat becomes slow. However, in terms of the micro-TBC, the high surface roughness and the high defects inside not only increase the contact of corrosive salt and Y element, but also make the molten salt easily penetrate into zirconia coat. After 300 h of corrosion, even the whole zirconia coating with thickness of 200 μm can be penetrated by molten salt [15]. Therefore, the application of nanostructured YSZ plays a same role in improving hot corrosion resistance as inert coating material and sealing treatment.

3.2 Phase transformation of ceramic coating induced by hot corrosion

It is evidenced that apparent phase transformation has been undergoing by comprehensive comparison of Figs. 1c and 4, i.e., the presence of the peaks located at 28.2 and 31.5° corresponding to the crystal orientations of $[11\bar{1}]$ and [111] of the monoclinic phase, respectively. The transformation from tetragonal phase to monoclinic phase accompanies stress evolution and it is unfavorable to the application of YSZ. Many reports summarized

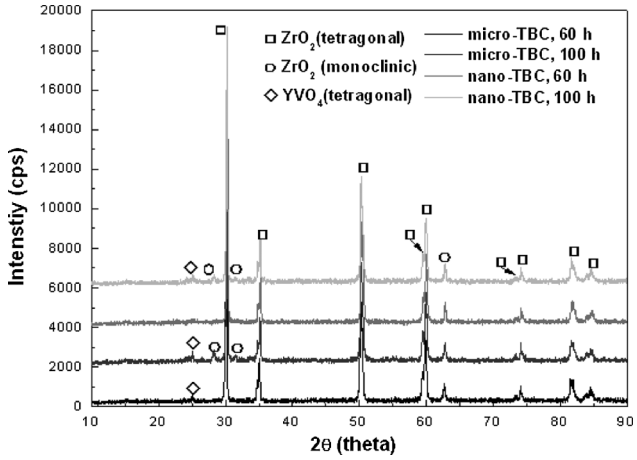

Figure 4. XRD patterns show the surface components after hot corrosion

by Ref. [6] have been focused on the above mentions, suggesting that temperature, particle size, crystallization atmosphere or defects have important effects. Although 8 wt% Y_2O_3 can stabilize the tetragonal phase, it cannot prevent the phase transformation in the practical application. The typical case is that hot corrosion can result in the phase transformation [15, 16, 30]. It is attributed to the consumption of yttrium, and thereby the stabilizing effect is reduced.

A simple method to identify the extent of phase transformation has been developed by comparing the different XRD peak intensities. The volume fraction of monoclinic phase in the coating (m%) can be estimated by the following equation [16, 30, 39, 40]:

$$\mathrm{m}\% = \frac{I_\mathrm{m}(\bar{1}11) + I_\mathrm{m}(111)}{I_\mathrm{m}(\bar{1}11) + I_\mathrm{m}(111) + I_\mathrm{t}(111)} \times 100\% \quad (4)$$

where I_m is the intensity of monoclinic peaks, I_t is the intensity of tetragonal peaks. Figure 5 shows the volume fractions of monoclinic phase in both coatings before and after hot corrosion calculated according to equation (4). The m% of both as-sprayed coatings was about 4.4%. After 60 h of hot corrosion, the m% of micro-TBC increased to 5.3%, which is somewhat higher than nano-TBC of 4.8%. Up to 100 h, both the m% of coatings increase and the difference between micro-TBC and nano-TBC increased. The monoclinic fraction after 100 h oxidation of the micro-TBC (8.6%) was much higher than nano-TBC (6.7%). This reveals that the transformation from tetragonal phase to monoclinic phase occurred. In order to further identify that the phase transformation is induced by hot corrosion, an aging/isothermal oxidation test at the same temperature for 100 h was carried out. The m% calculated by equation (4) of both coatings was 4.6 and 5.1%, respectively. These values are similar with that of as-sprayed coatings, which indicates that isothermal oxidation limited to 100 h has no effect on the phase transformation. Above mentions imply that hot corrosion is the only factor determining the phase transformation at 900 °C. The nano-TBC displays a better resistance to phase transformation induced by hot corrosion.

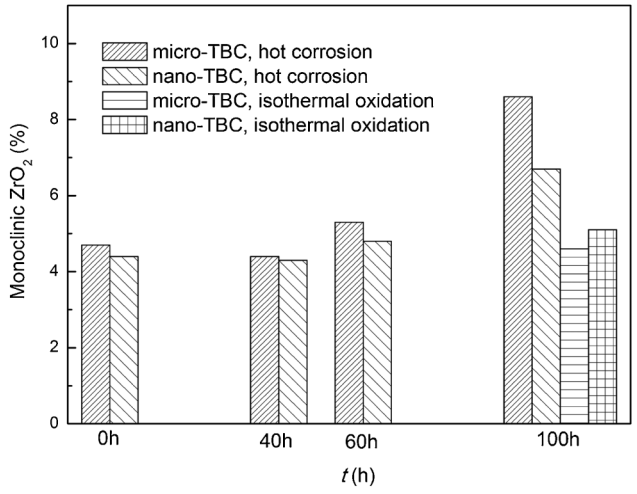

Figure 5. Volume fraction of monoclinic phase in the coatings before and after hot corrosion or isothermal oxidation

4 Conclusions

In the present investigation, the comparison of hot corrosion behaviors between nanostructured and microstructured TBCs under the surroundings of Na_2SO_4 and V_2O_5 salt at 900 °C has been carried out. It is concluded that the nanostructured TBCs were more resistant to hot corrosion than the microstructured TBCs due to nanocrystallization. Based on XRD quantitative analysis, the nanostructured TBCs were evidenced to have a better resistance to the tetragonal-monoclinic phase transformation.

Acknowledgements: This work was supported by National Natural Science Foundation of China (no. 51010005, 90916020) and the Program for New Century Excellent Talents in University (NCET-08-0168).

5 References

[1] Carlos. G. Levi, *Curr. Opin. Solid State Mater. Sci.* **2004**, *8*, 77.
[2] J. Nicholls, *MRS Bull.* **2003**, *28*, 659.
[3] R. B. Heimann, *Adv. Ceram. Mater.* **1996**, *122*, 399.
[4] B. Goswami, A. K. Ray, S. K. Sahay, *High Temp. Mater. Proc.* **2004**, *23*, 73.
[5] X. Q. Cao, R. Vassen, D. Stoever, *J. Eur. Ceram. Soc.* **2004**, *24*, 1.
[6] X. Q. Cao, *Materials for Thermal Barrier Coatings*, Science Press, Beijing **2007**.
[7] A. Feuerstein, J. Knapp, T. Taylor, A. Ashary, A. Bolcavage, N. Hitchman, *J. Therm. Spray Technol.* **2008**, *17*, 199.
[8] M. P. Taylor, H. E. Evans, S. Gray, J. R. Nicholls, *Mater. Corros.* **2011**, *62*, 668.
[9] A. G. Evans, D. R. Mumm, J. W. Hutchinson, G. H. Meier, F. S. Pettit, *Prog. Mater. Sci.* **2001**, *46*, 505.
[10] N. P. Padture, M. Gell, E. H. Jordan, *Science* **2002**, *296*, 280.
[11] B. Gleeson, *J. Propul. Power.* **2006**, *22*, 375.
[12] M. A. Helminiak, N. M. Yanar, F. S. Petit, T. A. Taylor, G. H. Meier, *Mater. Corros.* **2012**, *63*, 929.

[13] D. R. Clarke, C. G. Levi, *Annu. Rev. Mater. Res.* **2003**, *33*, 383.
[14] C. H. Lee, H. K. Kim, H. S. Choi, H. S. Ahn, *Surf. Coat. Technol.* **2000**, *124*, 1.
[15] S. Y. Park, J. H. Kim, M. C. Kim, H. S. Song, C. G. Park, *Surf. Coat. Technol.* **2005**, *190*, 357.
[16] Z. H. Xu, L. M. He, R. D. Mu, S. M. He, G. H. Huang, X. Q. Cao, *Surf. Coat. Technol.* **2010**, *204*, 3652.
[17] R. A. Miller, *Surf. Coat. Technol.* **1987**, *30*, 1.
[18] G. C. Chang, W. Phucharoen, R. A. Miller, *Surf. Coat. Technol.* **1987**, *30*, 13.
[19] W. Hertl, *J. Appl. Phys.* **1988**, *63*, 5514.
[20] R. L. Jones, *J. Therm. Spray Technol.* **1997**, *6*, 77.
[21] R. Srinivasan, J. M. Merrilea, *Surf. Coat. Technol.* **2002**, *160*, 187.
[22] R. L. Jones, *J. Am. Ceram. Soc.* **1992**, *75*, 1818.
[23] B. A. Nagaraj, D. J. Wortman, *J. Eng. Gas Turbines Powder* **1990**, *112*, 536.
[24] S. Li, Z. G. Liu, J. H. Ouyang, *Corros. Sci.* **2010**, *52*, 3568.
[25] G. Sreedhar, V. S. Raja, *Corros. Sci.* **2010**, *52*, 2592.
[26] X. Zhong, Y. Wang, Z. Xu, Y. Zhang, J. Zhang, X. Cao, *Mater. Corros.* **2009**, *60*, 882.
[27] B. Liang, C. X. Ding, H. L. Liao, C. Coddet, *Surf. Coat. Technol.* **2006**, *200*, 4549.
[28] B. Liang, C. X. Ding, *Surf. Coat. Technol.* **2005**, *197*, 185.
[29] R. S. Lima, A. Kucuk, C. C. Berndt, *Surf. Coat. Technol.* **2001**, *135*, 166.
[30] A. Abbas, S. Mohsen, K. Akira, *Mater. Sci. Eng.* **2008**, *A478*, 264.
[31] R. L. Jones, C. E. Williams, S. R. Jones, *J. Electrochem. Soc.* **1986**, *133*, 227.
[32] C. Batista, A. Portinha, R. M. Ribeiro, V. Teixeira, C. R. Oliveira, *Surf. Coat. Technol.* **2006**, *200*, 6783.
[33] S. Li, Z. G. Liu, J. H. Ouyang, *Mater. Corros.* **2012**, *63*, 303.
[34] J. C. Hamilton, A. S. Nagellerg, *J. Am. Ceram. Soc.* **1984**, *67*, 686.
[35] Z. Chen, N. Q. Wu, J. Singh, S. X. Mao, *Thin Solid Films* **2003**, *443*, 46.
[36] R. S. Lima, B. R. Marple, *J. Therm. Spray Technol.* **2008**, *17*, 846.
[37] H. Zhou, F. Li, J. Wang, B. D. Sun, *J. Coat. Technol. Res.* **2009**, *6*, 3830.
[38] X. L. Jiang, C. B. Liu, F. Lin, *J. Mater. Sci. Technol.* **2007**, *23*, 449.
[39] H. Toraya, M. Yoshimura, S. Somiya, *J. Am. Ceram. Soc.* **1984**, *67*, 183.
[40] J. R. Brandon, R. Taylor, *Surf. Coat. Technol.* **1991**, *46*, 75.

(Received: March 6, 2012) W6571
(Accepted: August 3, 2012)

